Reduction of the mathematical model of liquid flow within an instability

IOP Conf. Series: Earth and Environmental Science **240** (2019) 072026 doi:10.1088/1755-1315/240/7/072026

Reduction of the mathematical model of liquid flow within an instability

F Pochylý, O Urban and S Fialová[1]

Brno University of Technology, Energy Institute, Viktor Kaplan Department of Fluid Engineering, Technická 2896/2, 616 69 Brno, Czech Republic

[1] e-mail: fialova@fme.vutbr.cz

Abstract. The instability of stationary vortex structures is manifested by an oscillation at several fundamental frequencies which are associated with characteristic shapes. It is caused by the nonlinear convective terms in the Navier-Stokes equations. The frequency of unstable oscillation can be detected by the Fourier transform of the velocity and the pressure field themselves or their constitutive modes. It is this knowledge of the constitutive modes that is the basis for using the inverse method to define a reduced mathematical model in a finite-dimensional space. This model allows to analyze the vortex structures in the region of instability and their dependence on inhomogeneous boundary conditions. Present paper describes the essential steps of deriving an inverse method. The inverse method is applied to fluid flow in the draft tube of a swirl generator. The dynamic mode decomposition and the discrete Fourier transform of the flow field are assessed as possible methods that can provide the modal and spectral matrix for the model.

1. Introduction

The subject of this article is a simplified mathematical model allowing an analysis of vortex structures in liquid flow and their elimination by external forcing. Unsteady vortex structures result from a loss of stability of a steady flow. The essence of unsteady liquid behavior is to be found in the convective terms of the Navier-Stokes equations and their dependence on the boundary conditions [1]. In the search for the causes of the instability, linearized Navier-Stokes equations can be used. In such modified equations, the convective terms are heavily dependent on the steady flow velocity $\boldsymbol{v}_0(\boldsymbol{x}, t)$. For small values of velocity and pressure and appropriate boundary conditions, the irreversible stress tensor can dominate over the convective terms and the liquid flow is steady. When increasing the liquid velocity, the asymmetric part of the convective terms prevails and unsteady vortex structures are formed. It should be noted that the asymmetric part of the convective terms is dependent on the boundary conditions. Appropriate boundary conditions can significantly affect the stability of the flow.

The following analysis is focused on a linear model that describes the fluctuating components of liquid velocity and pressure. The mathematical model is based on a modal decomposition of turbulent velocity and pressure field. As a test case, the flow in the draft tube of a swirl generator was selected. It exhibits a spiralling vortical structure, the so-called vortex rope. Mitigation of the vortex rope in Francis turbines is desirable as it affects the opperating range of these machines, and is still a subject of research. Two decomposition methods are investigated – the discrete Fourier transform (DFT) and the dynamic mode decomposition (DMD). Their dimensionality reduction performance is also assessed by comparison with the energetically optimal proper orthogonal decomposition. Low-dimensionality is a key aspect of nonlinear reduced-order models for flow control, which are out of the scope of this paper.

2. Mathematical model

Let a vector $\boldsymbol{w}$ be composed of the components of velocity and pressure at selected points of the computational domain in time t. So $\boldsymbol{w}^{\mathrm{T}} = \left(\boldsymbol{v}^{\mathrm{T}}, \boldsymbol{p}^{\mathrm{T}}\right)$. Consider an incompressible Newtonian liquid. For a discretized spatial domain, the linearized Navier-Stokes equations can be written in the form

$$\boldsymbol{M}\frac{\mathrm{d}\boldsymbol{v}'}{\mathrm{d}t} + \boldsymbol{B}(\boldsymbol{v}_0)\boldsymbol{v}' + \boldsymbol{R}\boldsymbol{p}' = \boldsymbol{f}, \tag{2.1}$$

$$\boldsymbol{D}\boldsymbol{v}' = \boldsymbol{n}, \tag{2.2}$$

where the vectors $\boldsymbol{f}$ and $\boldsymbol{n}$ arise due to incorporation of external forcing. The apostrophe denotes the fluctuating component, i.e. the time-dependent deviation from the fixed point $\boldsymbol{w}_0^{\mathrm{T}} = \left(\boldsymbol{v}_0^{\mathrm{T}}, \boldsymbol{p}_0^{\mathrm{T}}\right)$. After some algebraic manipulation, this model can be written as

$$\frac{\mathrm{d}\boldsymbol{w}'}{\mathrm{d}t} + \boldsymbol{P}\boldsymbol{w}' = \boldsymbol{g}. \tag{2.3}$$

We assume a purely oscillatory $\boldsymbol{w}'$, in which case the operator $\boldsymbol{P}$ is antisymmetric and has the form

$$\boldsymbol{P} = \begin{bmatrix} \boldsymbol{B} & \boldsymbol{R} \\ \boldsymbol{D} & \boldsymbol{L} \end{bmatrix}. \tag{2.4}$$

Consider the eigenvalue problem for the matrix $\boldsymbol{P}$ and its complex conjugate transpose $\boldsymbol{P}^*$

$$\boldsymbol{P}\boldsymbol{X} - \boldsymbol{X}\boldsymbol{S} = 0 \tag{2.5}$$

$$\boldsymbol{P}^*\boldsymbol{Y} - \boldsymbol{Y}\boldsymbol{\Theta} = 0. \tag{2.6}$$

The following relations can be derived:

$$\boldsymbol{Y}^*\boldsymbol{X} = \boldsymbol{I}, \qquad \boldsymbol{Y}^*\boldsymbol{P}\boldsymbol{X} = \boldsymbol{S}. \tag{2.7}$$

The modal matrices $\boldsymbol{X}$, $\boldsymbol{Y}$ can be divided into the velocity part $\boldsymbol{X}_v$, $\boldsymbol{Y}_v$ and the pressure part $\boldsymbol{X}_p$, $\boldsymbol{Y}_p$

$$\boldsymbol{X} = \begin{bmatrix} \boldsymbol{X}_v \\ \boldsymbol{X}_p \end{bmatrix}, \qquad \boldsymbol{Y} = \begin{bmatrix} \boldsymbol{Y}_v \\ \boldsymbol{Y}_p \end{bmatrix}. \tag{2.8}$$

Since the operator $\boldsymbol{P}$ is antisymmetric, the eigenvalues are purely imaginary and paired. The eigenvectors are paired as well. With a known modal and spectral matrix, the operator $\boldsymbol{P}$ can be reconstructed based on the following relations:

$$\boldsymbol{B} = \boldsymbol{X}_v\boldsymbol{S}\boldsymbol{Y}_v^*, \qquad \boldsymbol{R} = \boldsymbol{X}_v\boldsymbol{S}\boldsymbol{Y}_p^*, \tag{2.9}$$

$$\boldsymbol{D} = \boldsymbol{X}_p\boldsymbol{S}\boldsymbol{Y}_v^*, \qquad \boldsymbol{L} = \boldsymbol{X}_p\boldsymbol{S}\boldsymbol{Y}_p^*. \tag{2.10}$$

The matrix $\boldsymbol{Y}^*$ can be computed from (2.7) using the inverse matrix $\boldsymbol{X}^{-1}$

$$\boldsymbol{Y}^* = \boldsymbol{X}^{-1}. \tag{2.11}$$

The solution of the linear system (2.3) based on the modal decomposition (2.5) has the form

$$\boldsymbol{w}'(t) = \boldsymbol{X}\boldsymbol{\Gamma}(t)\boldsymbol{X}^{-1}\boldsymbol{w}(0) + \boldsymbol{X}\int_0^t \boldsymbol{\Gamma}(t-\tau)\boldsymbol{X}^{-1}\boldsymbol{g}(\tau)d\tau, \tag{2.12}$$

where $\boldsymbol{\Gamma}(t)$ is the spectral matrix exponential

$$\boldsymbol{\Gamma}(t) = \exp(\boldsymbol{S}t). \tag{2.13}$$

If the dynamics are dominated by coherent structures, most of the modes are negligible. The modal matrix $\boldsymbol{X}$ is after their omission no longer square and the inverse matrix must be replaced by the pseudoinverse matrix $\boldsymbol{X}^{\dagger}$:

$$\boldsymbol{w}'(t) = \boldsymbol{X}\boldsymbol{\Gamma}(t)\boldsymbol{X}^{\dagger}\boldsymbol{w}(0) + \boldsymbol{X}\int_0^t \boldsymbol{\Gamma}(t-\tau)\boldsymbol{X}^{\dagger}\boldsymbol{g}(\tau)d\tau. \tag{2.14}$$

The main advantage of linear models is the knowledge of the solution in closed form including external forcing, so the time dependence of the vortex structures can be studied directly using the relation (2.14). Thanks to it, the theory focused on the determination of control laws is well-developed. Here, we present a method which enables to instantly eliminate a selected pair of modes from the dynamics. Consider external forcing $\boldsymbol{g}(\tau)$ in the form

$$\boldsymbol{g}(\tau) = \boldsymbol{g}_0 \exp(-\mathrm{i}\Omega\tau). \tag{2.15}$$

Plugging this expression into (2.14) leads to

$$\boldsymbol{w}(t) = \boldsymbol{X}\boldsymbol{\Gamma}(t)\boldsymbol{X}^{\dagger}\boldsymbol{w}(0) + \boldsymbol{X}\left(\int_0^t \boldsymbol{\Gamma}(t-\tau)\exp(-\mathrm{i}\Omega\tau)d\tau\right)\boldsymbol{X}^{\dagger}\boldsymbol{g}_0. \tag{2.16}$$

The integrand has the form

$$\boldsymbol{\Gamma}(t-\tau)\exp(-\mathrm{i}\Omega\tau) = \begin{bmatrix} \exp(-\mathrm{i}(\Omega-\omega_1)\tau - \mathrm{i}\omega_1 t) & 0 & 0 \\ 0 & \ddots & 0 \\ 0 & 0 & \exp(-\mathrm{i}(\Omega-\omega_M)\tau - \mathrm{i}\omega_M t) \end{bmatrix}. \tag{2.17}$$

After integration we obtain

$$\int_0^t \exp(-\mathrm{i}(\Omega-\omega)\tau - \mathrm{i}\omega t)d\tau = \frac{\exp(-\mathrm{i}\Omega t) - \exp(-\mathrm{i}\omega t)}{-\mathrm{i}(\Omega-\omega)}. \tag{2.18}$$

Let a matrix $\boldsymbol{C}$ be defined as follows

$$\boldsymbol{C} = \begin{bmatrix} \dfrac{1}{-\mathrm{i}(\Omega-\omega_1)} & 0 & 0 \\ 0 & \ddots & 0 \\ 0 & 0 & \dfrac{1}{-\mathrm{i}(\Omega-\omega_M)} \end{bmatrix}. \tag{2.19}$$

Using this matrix, equation (2.16) can be rewritten

$$\boldsymbol{w}(t) = \boldsymbol{X}\left(\boldsymbol{\Gamma}(t)\boldsymbol{X}^{\dagger}\boldsymbol{w}(0) + \boldsymbol{C}\boldsymbol{X}^{\dagger}\boldsymbol{g}_0\exp(-\mathrm{i}\Omega t) - \boldsymbol{\Gamma}(t)\boldsymbol{C}\boldsymbol{X}^{\dagger}\boldsymbol{g}_0\right) = \boldsymbol{X}\boldsymbol{h}(t), \tag{2.20}$$

where $\boldsymbol{h}(t)$ is a time-dependent $M \times 1$ vector. Since the modal matrix $\boldsymbol{X}$ is composed of paired modes, to eliminate a given pair, the following condition must be satisfied:

$$\boldsymbol{x}_k h_k(t) + \boldsymbol{x}_{k+1} h_{k+1}(t) = 0, \tag{2.21}$$

where $\boldsymbol{x}_k$ denote the k-th column of the matrix $\boldsymbol{X}$ and $h_k(t)$ denote the k-th element of the vector $\boldsymbol{h}(t)$. This condition ensures that the selected pair of modes does not contribute to the resultant dynamics. Let us analyze the structure of $h_k(t)$. With the known structures of the matrices $\boldsymbol{\Gamma}(t)$ and $\boldsymbol{C}$, the following expression can be obtained

$$h_k(t) = \exp(-\mathrm{i}\omega_k t)\boldsymbol{x}_k^{\dagger}\boldsymbol{w}(0) + \left[\frac{\exp(-\mathrm{i}\Omega t) - \exp(-\mathrm{i}\omega_k t)}{-\mathrm{i}(\Omega-\omega_k)}\right]\boldsymbol{x}_k^{\dagger}\boldsymbol{g}_0, \tag{2.22}$$

where $\boldsymbol{x}_k^{\dagger}$ denote the k-th row of the pseudoinverse matrix $\boldsymbol{X}^{\dagger}$. To avoid forced oscillation, from this point on, we assume steady forcing, i.e. $\Omega = 0$. In this case, the expression reduces to

$$h_k(t) = \exp(-\mathrm{i}\omega_k t)\left(\boldsymbol{x}_k^{\dagger}\boldsymbol{w}(0) - \frac{1}{\mathrm{i}\omega_k}\boldsymbol{x}_k^{\dagger}\boldsymbol{g}_0\right). \tag{2.23}$$

Furthermore, we introduce the following expressions

$$\boldsymbol{x}_k = \boldsymbol{a} + \boldsymbol{b}\mathrm{i}, \tag{2.24}$$

$$\boldsymbol{x}_{k+1} = \boldsymbol{a} - \boldsymbol{b}\mathrm{i}, \tag{2.25}$$

$$\boldsymbol{x}_k^\dagger = \boldsymbol{c} + \boldsymbol{d}\mathrm{i}, \tag{2.26}$$

$$\boldsymbol{x}_{k+1}^\dagger = \boldsymbol{c} - \boldsymbol{d}\mathrm{i}. \tag{2.27}$$

With $\omega_{k+1} = -\omega_k$, plugging the expressions (2.23)–(2.27) into the condition (2.21) yields the following conditions

$$\boldsymbol{c}\boldsymbol{w}(0) - \frac{1}{\omega_k}\boldsymbol{d}\boldsymbol{g}_0 = 0, \tag{2.28}$$

$$\boldsymbol{d}\boldsymbol{w}(0) + \frac{1}{\omega_k}\boldsymbol{c}\boldsymbol{g}_0 = 0. \tag{2.29}$$

The external forcing $\boldsymbol{g}_0$ must satisfy these two conditions. In that case, the selected pair of modes is suppressed.

Another and more common way to mitigate the dynamics is to design a closed-loop controller. Consider for example proportional control

$$\boldsymbol{g} = \boldsymbol{K}\boldsymbol{w}'. \tag{2.30}$$

Plugging into the equation (2.3) yields

$$\frac{\mathrm{d}\boldsymbol{w}'}{\mathrm{d}t} = (\boldsymbol{K} - \boldsymbol{P})\boldsymbol{w}'. \tag{2.31}$$

The task is to construct the matrix $\boldsymbol{K}$ so that all eigenvalues of the matrix $\boldsymbol{K} - \boldsymbol{P}$ have a negative real part. In such case, the dynamics are stable which means that the fluctuations will eventually fade out.

3. Vortex rope

The subject of this part is a spiralling vortical structure, the so-called vortex rope. This phenomenon is present in the draft tube of Francis turbines and significantly affects the operating range of these machines. It is therefore desirable to mitigate the instability by means of external forcing.

For the purposes of experimental investigations, the vortex rope is usually generated by a swirl generator. It is a simple device that generates tangential velocity at the inlet of its draft tube so that the instability is formed. Our generator has two separate inlets (axial and tangential). This enables to set different ratios of axial to tangential velocity and hence to investigate the dependence of the vortex rope on the operating point. The geometry of the device is sketched in figure 1.

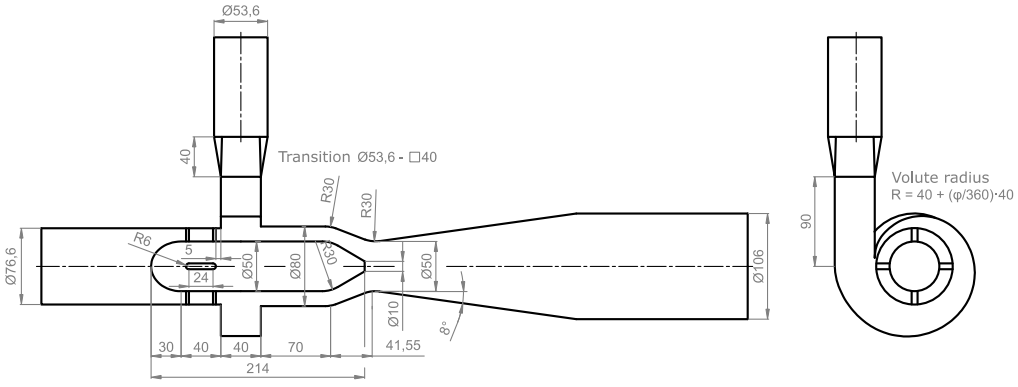

Figure 1. Swirl generator apparatus.

The selected operating point for this study is given by the total flow rate of 10 liters of water per second from which thirty percent comes through the axial inlet and the rest comes through the tangential inlet. With these conditions, the flow field in the draft tube is similar to that in Francis turbines operating in part load [2].
The aim of this study is to find surrogate linear models from data. The vector $\boldsymbol{w}$ composed of $M = 300$ snapshots of the velocity and the pressure field was obtained by CFD simulation of the Reynolds-averaged Navier-Stokes equations and the Reynolds stress equation model for the computation of the Reynolds stress tensor components. During this period, the resultant vortex rope turns around the axis of the draft tube 14 times. It should be noted that the assumptions of the linearized governing equation (i.e. close vicinity of the fixed point) are not satisfied here so linear models are not physical. However, they can still be valuable as a guide for the determination of candidate control laws. The utilization of linear models is motivated by the existence of the solution in closed form and also by the Koopman theory, which states that sufficiently rich measurements of a nonlinear system can be advanced in time by a linear Koopman operator [3], [4].
We investigate two methods that provide a modal decomposition in the same form as the approximate solution of linear models (2.14) – the dynamic mode decomposition (DMD) and the discrete Fourier transform (DFT). It should be noted that a connection exists between these methods. As Chen et al. pointed out, subtracting the ensemble average from the data exactly reduces DMD to DFT which is typically undesirable [5]. Therefore, we applied DMD to the raw data. The purpose is to determine whether the vortex rope phenomenon is reducible, i.e. whether only a few modes are enough to capture the important dynamics. This is important for the construction of physical nonlinear reduced-order models and their possible utilization in control [6], [7]. As both DMD and DFT are constrained by single frequency per mode, we compare their performance to the unconstrained energetically optimal proper orthogonal decomposition (POD).

3.1 CFD results

In the following, we concentrate on the pressure field since it is a good quantity for visualizations of the vortex rope (low pressure area induced by the rotating motion) and the amplitude of the pressure pulsations has direct impact on the operating range of Francis turbines.
For the decompositions, data only from the draft tube were used. A weighted average of the frequency spectra was computed from the following relation:

$$A_{\mathrm{w}}(f_n) = \frac{1}{\frac{1}{2}\rho v^2} \frac{\sum_i (A(f_n, x_i) V_i \sum_n A(f_n, x_i))}{\sum_i (V_i \sum_n A(f_n, x_i))}, \tag{3.1}$$

where $A_{\mathrm{w}}(f_n)$ is a dimensionless weighted amplitude corresponding to the frequency f_n. Cells of the computational grid with a larger volume (V_i is the cell volume) and a higher sum of amplitudes of all frequencies are stressed more. $\boldsymbol{x}_i = (x_i, y_i, z_i)$ is the location of the cell center. The reference velocity v is given by

$$v = \frac{Q}{S_{\mathrm{ld}}}, \tag{3.2}$$

where S_{ld} is the area of the cross section of the draft tube with the lowest diameter (i.e. 50 mm in this case). The amplitudes serve as a measure of importance of each frequency. The weighted frequency spectrum is depicted in figure 2. together with visualizations of the vortex rope at three different time instants. The structure was made visible by means of the volume rendering method. Regions with high pressures, which are out of interest, were made transparent. The sharp transition from blue to yellow in the colormap unveils complicated vortical structures (yellow) in the main spiralling structure (blue). The predominant motion of the structure is a precession around the axis of the draft tube. Consequently, the most dominant frequencies and their corresponding modes are associated with the precessing motion.

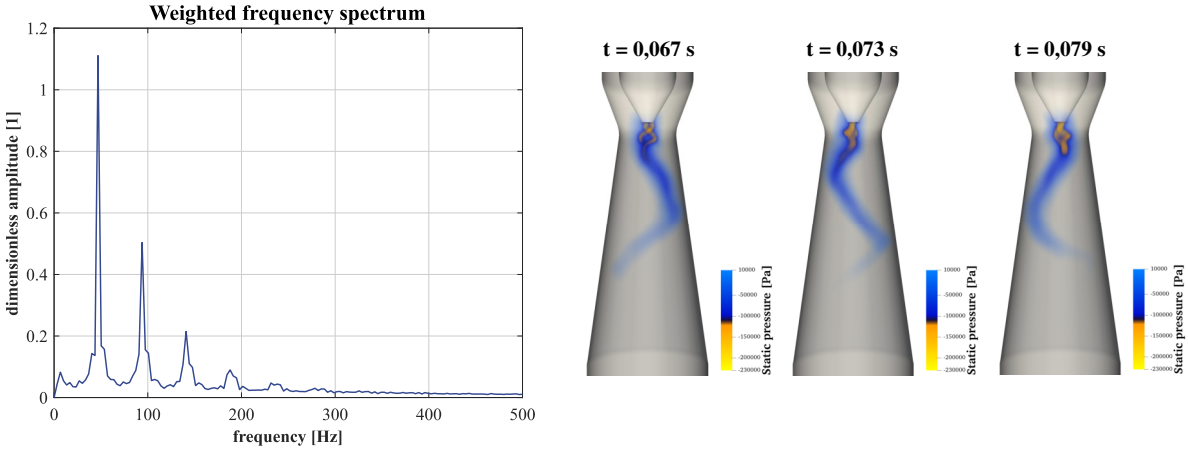

Figure 2. Weighted frequency spectrum of the fluctuations of static pressure and pictures of the vortex rope at different time instants visualized by a volume rendering of the static pressure field. Higher values were made transparent so that only the low-pressure region induced by the vortex rope is visible.

3.2 Dynamic mode decomposition

The DMD was introduced by Schmid [8] as a method of computation of the best-fit linear operator $\boldsymbol{A}$ which advances measurements of the system in time

$$\boldsymbol{W}' = \boldsymbol{A}\boldsymbol{W}, \tag{3.3}$$

where the k-th column of the matrix $\boldsymbol{W}'$ equals to the $k+1$-st column of the matrix of measurements $\boldsymbol{W}$. Since the operator $\boldsymbol{A}$ is of $N \times N$ dimension, i.e. usually too large, DMD computes a matrix $\tilde{\boldsymbol{A}}$ instead, which is related to the matrix $\boldsymbol{A}$ using the singular value decomposition modes of the matrix $\boldsymbol{W}$

$$\boldsymbol{W} = \boldsymbol{U}\boldsymbol{\Sigma}\boldsymbol{V}^{\mathrm{T}}, \tag{3.4}$$

$$\tilde{\boldsymbol{A}} = \boldsymbol{U}^{\mathrm{T}}\boldsymbol{W}'\boldsymbol{V}\boldsymbol{\Sigma}^{-1}. \tag{3.5}$$

The DMD modal and spectral matrices are given by the eigenvalue problem of $\tilde{\boldsymbol{A}}$

$$\tilde{\boldsymbol{A}}\boldsymbol{\phi} = \boldsymbol{\phi}\boldsymbol{S}_{\mathrm{DMD}}, \tag{3.6}$$

where the modal matrix is computed from the matrix $\boldsymbol{\phi}$ as follows:

$$\boldsymbol{X}_{\mathrm{DMD}} = \boldsymbol{W}'\boldsymbol{V}\boldsymbol{\Sigma}^{-1}\boldsymbol{\phi}. \tag{3.7}$$

3.3 Discrete Fourier transform

The DFT is a classical method which decomposes the input signal into harmonic components with zero decay/growth rate [9]. The elements of the modal matrix are given by

$$\hat{X}_{\mathrm{DFT}(jk)} = \sum_{n=0}^{M-1} W_{j(n+1)} \cdot \exp\left[-\frac{2\pi \mathrm{i}}{T}\left(k - \frac{M}{2}\right) t_{n+1}\right], \tag{3.8}$$

if M is even. Next, we normalize each column of $\hat{\boldsymbol{X}}_{\mathrm{DFT}}$ denoted as $\hat{\boldsymbol{x}}_{\mathrm{DFT}(i)}$

$$\boldsymbol{x}_{\mathrm{DFT}(i)} = \frac{\hat{\boldsymbol{x}}_{\mathrm{DFT}(i)}}{\left\|\hat{\boldsymbol{x}}_{\mathrm{DFT}(i)}\right\|} = \frac{\hat{\boldsymbol{x}}_{\mathrm{DFT}(i)}}{\left[\hat{\boldsymbol{x}}^{*}_{\mathrm{DFT}(i)} \cdot \hat{\boldsymbol{x}}_{\mathrm{DFT}(i)}\right]^{1/2}}. \tag{3.9}$$

The spectral matrix $\boldsymbol{S}_{DFT}$ is a diagonal matrix. Consider a vector $\boldsymbol{s}$ which contains the diagonal elements of the spectral matrix. It is given by

$$s_k = -\frac{2\pi \mathrm{i}}{T}\left(k - \frac{M}{2}\right) \tag{3.10}$$

3.4 Proper orthogonal decomposition

The POD method was introduced into fluid mechanics by Lumley [10]. The idea is to decompose the flow field into a set of modes optimal in the ℓ^2 norm. It is in fact equivalent to the SVD of $\boldsymbol{W}$

$$\boldsymbol{W} = \boldsymbol{X}_{\mathrm{POD}}\boldsymbol{\Lambda}\boldsymbol{V}_{\mathrm{POD}}^{\mathrm{T}}. \tag{3.11}$$

The singular values in $\boldsymbol{\Lambda}$ are equivalent to the ℓ^2 norm of the modes squared, and serve as a measure of their importance.

3.5 Results

The most important modes connected with the precessing motion are depicted in figure 3. The spatial shapes are very similar for all decompositions. Differences among the methods can be seen in the temporal evolutions of the modes. Only POD takes the changes of the amplitudes in time into account. DMD can account for purely decaying or growing evolutions only, which is not the case here. The small decay of the first DMD mode can be eliminated if more data are used. The most important drawback of DFT is that it assumes periodical data. Temporal evolutions of non-periodical data exhibit unphysical jumps between the last and the first value as the covered range starts to repeat. DMD temporal evolutions will, on the other hand, eventually suffer from nonzero real parts of the diagonal elements of the spectral matrix. This should be taken into account when using models based on DFT or DMD.

The dimensionality reduction potential of the three methods can be assessed using the squared ℓ^2 norm of the modes. For POD, this is obtained readily as it equals to the singular values $\boldsymbol{\Lambda}$. For the rest two methods, the corresponding values need to be computed. We define a matrix of the temporal evolution of the j-th mode. Its columns are given by

$$\boldsymbol{z}_i = \boldsymbol{x}_j e^{S_{jj}t_i}\boldsymbol{x}_j^{\dagger}\boldsymbol{w}(0). \tag{3.12}$$

The corresponding parameter Λ_j is then computed from the following expression

$$\Lambda_j = \|\mathrm{real}(\boldsymbol{Z})\|^2, \tag{3.13}$$

where the Frobenius norm is used. This algorithm is valid for both DFT and DMD. We note that the parameter $\boldsymbol{\Lambda}$ is for velocity data proportional to kinetic energy. This is why POD is called energetically optimal.

The chart in figure 5 shows the accuracy of the reconstruction of the flow field using a given number of the most dominant modes classified by $\boldsymbol{\Lambda}$. POD is by definition the best. However, tens or even hundreds of modes need to be kept for a good accuracy. The effects of the unresolved scales need to be taken into account in nonlinear models. DFT initially outperforms DMD, but the situation gets reversed later.

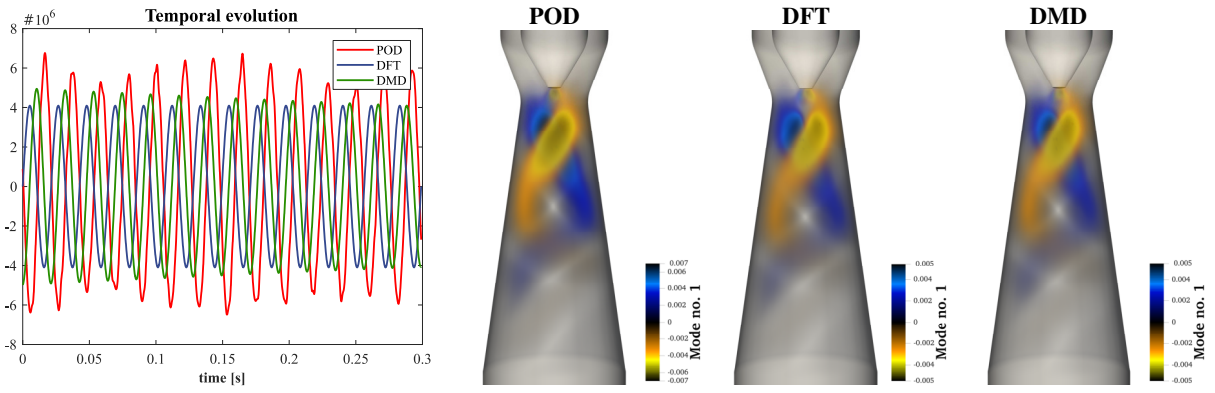

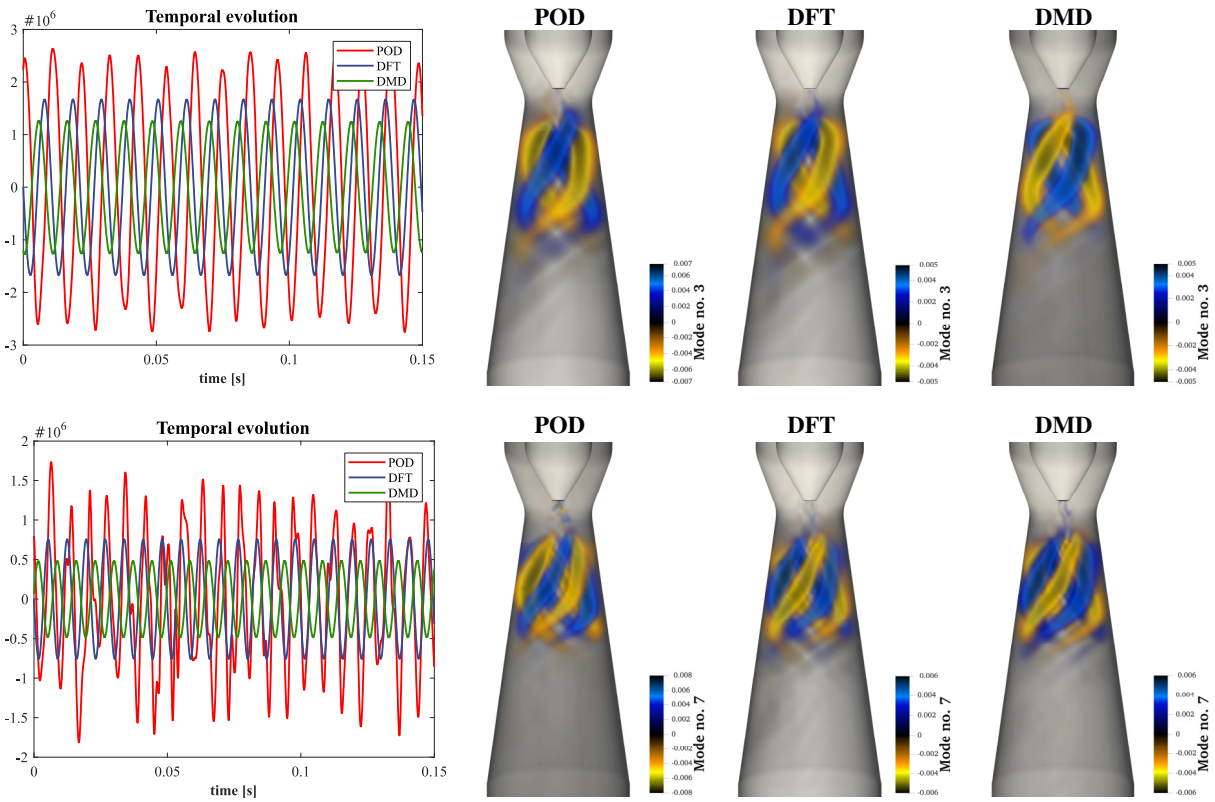

Figure 3. The most dominant modes of the vortex rope.

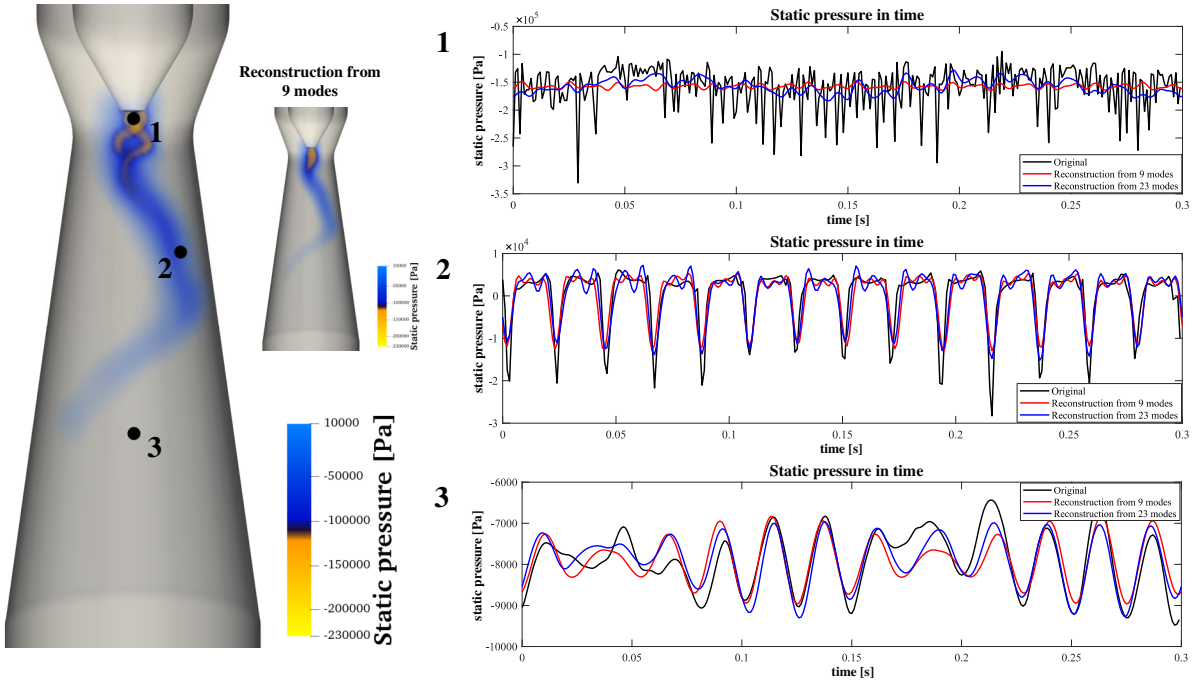

Figure 4. The dependency of static pressure on time for three distinct probes. Reconstructions are made from DFT modes classified using $\boldsymbol{\Lambda}$.

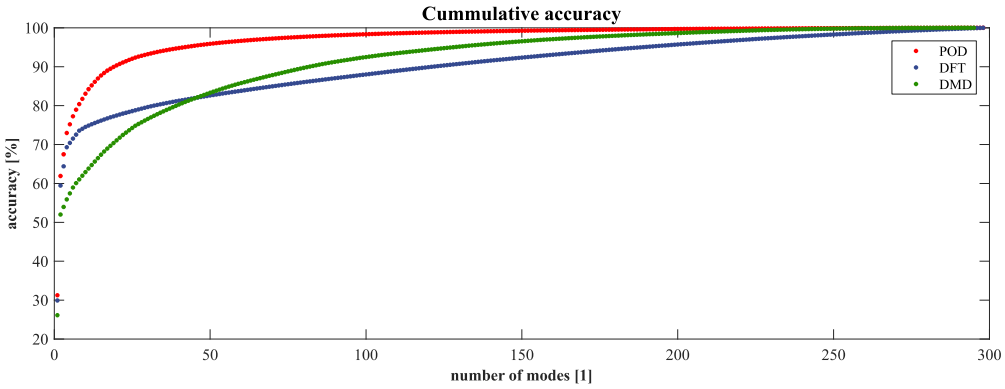

Figure 5. The accuracy of the reconstruction of the flow field from a given number of the most dominant modes in ℓ^2 norm.

The convergence curve of DFT exhibits a jump in the convergence rate – after 8 summed modes, the convergence rate gets suddenly much smaller. To find out the reasons, in figure 4 we compare the reconstructions from 9 and 23 modes to the original flow field. It is evident that 9 modes are enough to capture the main spiralling structure, but the complicated dynamics under the hub are poorly resolved in both cases. The poor performance is hence caused by the dynamics under the hub that exhibit many frequencies with comparable energy content.

4. Conclusion

In this paper, it has been shown that with knowledge of the modal and spectral matrix, it is possible to derive a linear model which can approximate the unsteady behavior of the part load vortex rope phenomenon. The matrices can be obtained from data by the discrete Fourier transform or the dynamic mode decomposition. Performance of these methods was compared with the energetically optimal POD method. As the investigated dynamics do not satisfy the assumptions of the linearized Navier-Stokes equations, the linear model serves only as a guide and nonlinear reduced-order models should be used in order to find proper control laws to mitigate the pressure pulsations. Such models have to be built on only a few number of modes. We conclude that the dynamics of the vortex rope are too complicated to be fully captured by such models, and so the effect of unresolved scales needs to be taken into account. Especially the structures right under the hub were found irreducible.

Acknowledgement

Grant Agency of the Czech Republic, within the projects GA101/17-01088S and GA101/17-19444S is gratefully acknowledged for support of this work.

References

[1] Pochylý F, Krausová H and Fialová S 2014 Application of the Shannon-Kotelnik theorem on the vortex structures identification *IOP Conf. Ser.: Earth Environ. Sci*. **22** 022023
[2] Wang H, Ruprecht A, Göde E and Riedelbauch S 2015 Analysis and control of the part load vortex rope in the draft tube of a pumpturbine 6*th IAHR meeting on the Working Group „Cavitation and Dynamic Problems in Hydraulic Machinery and Systems“*
[3] Koopman B O 1931 Hamiltonian systems and transformation in Hilbert space *PNAS* **17** pp 315–18
[4] Mezić I 2005 Spectral properties of dynamical systems, model reduction and decompositions *Non. Dyn.* **41** pp 309–25
[5] Chen K K, Tu J H and Rowley C W 2012 Variants of dynamic mode decomposition: boundary condition, Koopman, and Fourier analyses *J. Non. Sci* **22** pp 887–915

[6] Kerschen G, Golinval J C, Vakakis A F and Bergman L A. 2005 The method of proper orthogonal decomposition for dynamical characterization and order reduction of mechanical systems: an overview *Non. Dyn.* **41** pp 147–69
[7] Noack B R, Morzyński M and Tadmor G 2011 *Reduced-order modelling for flow control* (Udine: Springer)
[8] Schmid P J 2010 Dynamic mode decomposition of numerical and experimental data *J. Fluid Mech.* **656** pp 5–28
[9] Rosenfeld M 1995 Utilization of Fourier decomposition for analyzing time-periodic flows *Comp. Fluids* **24** pp 349–68
[10] Lumley J L *Atmospheric Turbulence and Radio Wave Propagation* (Moscow: Nauka)